

CERTIFICATE

It is certified that the work contained in the thesis titled "*Magnetic and Transport Properties of Spin Modulated Bulk and Heterostructured Quantum Materials*" by *Labanya Ghosh* has been carried out under my supervision and that this work has not been submitted elsewhere for a degree.

It is further certified that the student has fulfilled all the requirements of comprehensive examination, candidacy and SOTA for the award of Ph.D. Degree.



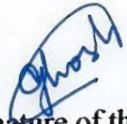
Prof. Sandip Chatterjee
(Supervisor)
Department of Physics,
Indian Institute of Technology,
Banaras Hindu University,
Varanasi-221005
Professor
Department of Physics
Indian Institute of Technology
(Banaras Hindu University)
Varanasi-221005

DECLARATION BY THE CANDIDATE

I, “*Labanya Ghosh*”, certify that the work embodied in this thesis is my own bonafide work and carried out by me under the supervision of “*Prof. Sandip Chatterjee*” from “*December 2017*” to “*December 2022*”, at the “*Department of Physics*”, Indian Institute of Technology (BHU), Varanasi. The matter embodied in this thesis has not been submitted for the award of any other degree/diploma. I declare that I have faithfully acknowledged and given credits to the research workers wherever their works have been cited in my work in this thesis. I further declare that I have not willfully copied any other's work, paragraphs, text, data, results, *etc.*, reported in journals, books, magazines, reports dissertations, theses, *etc.*, or available at websites and have not included them in this thesis and have not cited as my own work.

Date:


Place: IIT (BHU), Varanasi


Signature of the student


(*Labanya Ghosh*)

Certificate by the Supervisor

It is certified that the above statement made by the student is correct to the best of my knowledge.


Prof. Sandip Chatterjee
(Supervisor)
Professor

Department of Physics
Indian Institute of Technology
(Banaras Hindu University)
Varanasi-221005


Head of the Department
Department of Physics,
IIT (BHU), Varanasi

HEAD/विभागाध्यक्ष
भौतिकी विभाग/Deptt. of Physics
एच.प्रौ.सं./कां.हि.वि./IIT (BHU)
वाराणसी/Varanasi-221005

COPYRIGHT TRANSFER CERTIFICATE

Title of the Thesis: *Magnetic and Transport Properties of Spin Modulated Bulk and Heterostructured Quantum Materials*

Name of the Student: *Labanya Ghosh*

Copyright Transfer

The undersigned hereby assigns to the Indian Institute of Technology (Banaras Hindu University) Varanasi all rights under copyright that may exist in and for the above thesis submitted for the award of the “DOCTOR OF PHILOSOPHY”.

Date:

Place: IIT (BHU), Varanasi



Signature of the Student

(*Labanya Ghosh*)

Note: However, the author may reproduce or authorize others to reproduce material extracted verbatim from the thesis or derivative of the thesis for the author's personal use, provided that the source and the Institute's copyright notice are indicated.

Acknowledgement

The work presented in this thesis would not have been possible without my close association with many people who were always there when I needed them. I take this opportunity to acknowledge them and extend my sincere gratitude for helping me make this thesis a possibility. At this moment of accomplishment, first of all, I would like to pay homage to the founder of Banaras Hindu University, **Pandit Madan Mohan Malviya Ji**, who made this glorious temple to realize spiritual, technical, and scientific knowledge about this vast existing universe.

Even though this thesis' title page only mentions one name, innumerable people were involved in its acquisition. First and foremost, I want to express my gratitude to God Almighty for all His blessings and the opportunities He provided in my life. I would like to express my deepest gratitude to my supervisor **Professor Sandip Chatterjee** for allowing me to work in the field of Topological Quantum materials which is one of the most breakthrough discoveries in recent Condensed Matter Physics. I am really thankful to him for his trust, support, guidance, and scientific discussions throughout my Ph.D. career and for writing my thesis. Without his kind support, valuable time and cooperation, I would not have been able to complete my Ph.D. thesis successfully. His knowledge and the freedom of work he provided are commendable.

I appreciate and am thankful to my RPEC members, **Dr. Swapnil Patil** and **Dr. Somak Bhattacharyya**, for their knowledgeable, motivational, and umpteen suggestions throughout this research work. I want to express my deepest gratefulness to **Dr. Shiv Kumar** and **Dr. Prashant Shahi** for furnishing extraordinary measurement facilities abroad to execute the thesis work, without their support it could have been impossible to complete this thesis adequately. I express my gratefulness to **Prof. Prabhakar Singh** and **Prof. Debaprasad Giri** for their inspiration and support. I also wish to thank all the faculty members of the Department of Physics, IIT (BHU) Varanasi for their motivation, selfless support and suggestions during my Ph.D. time. I am also thankful to all the technical, non-teaching as well as office staff of the Department of Physics, IIT (BHU) Varanasi for their assistance when required. I would also like to thank CIFC, IIT (BHU) for providing experimental facilities during the entire course of research work.

I am thankful to the unknown reviewers who have rejected my papers several times in international conferences and journals. The comments that they provided helped to polish our articles in better shape. Nevertheless, the bigger and nobler cause of thanking them is that the rejections have equipped me with a high level of patience and helped me to exercise/implement my spiritual thoughts in practice. My acknowledgment will never be complete without the special mention of my lab seniors who have taught me the lab culture and have lived by example to make me understand the hard facts of life. My appreciation goes to my seniors and colleagues for their great help during my five years of the Ph.D. journey- **Dr. Abhishek Singh, Dr. Rahul Singh, Dr. Prince Gupta, Dr. Surajit Ghosh, Dr. Arkadeb Pal, Dr. Vinod Kumar Gangwar, Dr. Prajyoti Singh, Dr. Mahima Singh, Dr. Mohd Alam, Dr. Khyati Anand, Ms. Seema Kumari, Mr. Sambhab Dan, Ms. Srishti Dixit, Mr. Satya Vijay Kumar, Mr. Dheeraj Kumar, Ms. Neha Patel, Mr. Rahul Kumar Singh, Ms. Swayangsiddha Ghosh, Ms. Asmitha M, Mr. Nandkishor Pal, Sunil Verma, Ms. Sneha Yadav, Mr. Vishnu Sharma, Ms. Madhusmita Jena, Mr. Atul Kumar**

Acknowledgement

and **Mr. Shiv shakti Tiwari**. I like to give special thanks to my batchmates **Dr. Harshita Trivedi, Ms. Vagyashree Verma Mr. Prem Chandra Bharti, and Mr. Rajeshwar Prashad** with whom I started my journey at IIT (BHU), Varanasi. I convey my gratitude to all my teachers throughout my academic career for preparing me to walk through this long journey. All my friends from school to college, hostel life to academia- **Piyali, Priyanka, Debangana, Moutusi di, Moumita di, Payel, Bishnu, Arka, Anindita, Sathi, Smita**, and from the list is endless.... Thanks to all. Their association has made my journey a pleasurable and memorable experience. They were always beside me during the happy and hard moments to push me and motivate me. I am also thankful to all I could not mention here who helped me directly or indirectly throughout the work.

I am really amused being a part of a wonderful family. Recalling each and every person, fetching me a smile on my face. I always feel relaxed and pleased with their company- **Dida (Late Narmada Ghosh), Kaku (Mr. Suman Kalyan Ghosh), Kamma (Mrs. Dipanwina Ghosh), Barra Pisimoni (Sima Mandal), Barra Pisemosai (Late Manoranjan Mandal), Chhoto Pisimoni (Subha Dandapat), Chhoto Pisemosai (Bijay Dandapat), Mama, Mami, Masi, Mesomosai, Didima**. Though I am a single child, it never feels like that, as I have always been with these people- **Bubun da, Tubun da, Jhumpa di, Tukai, Piku, Aishi, Subha, Debi di**, and other cousins. I am indebted to all of them for their motivation, support and care during the journey of my life from a no-one to a Dr. Hereafter, I express my obligation to my second family- **my Parent in-laws (Mrs. Rekha Jana & Mr. Satyabrata Jana), Puja, Soumyajit da, Payel di** and other family members for their love, affection, and support during every moment of my life.

Last but not the least, words fail me to express my appreciation when it is time to share my gratitude to those very special people who always stood like a pillar of strength by my side, my parents- **Ma and Baba (Mrs. Rina Ghosh & Mr. Sumit Kumar Ghosh)**. Acknowledgment is a very small word in front of their contribution to my life and career because they are the oxygen of my life. They have always encouraged and motivated me to pursue an academic career with patience, hard work, sacrifice, ethics and honesty, which are the keywords to my success. Lastly, my solemn gratitude to the very important person in my life, my best friend, presently my life partner **Subhajit Jana** who stood by me no matter what. He was the one who used to pull me up when I was low and even get me back to the ground when flying high. His continuous support, unconditional love, excellent care and encouragement provided me the strength to win over all barriers and complete my work on time.

I gratefully acknowledge the **DST-INSPIRE** for providing me with the necessary funding and fellowship to pursue research work. Finally, I am grateful to Almighty for giving me the patience to make this endeavor a success.



Labanya Ghosh

*Dedicated to my beloved
Ma & Baba*

*“When you want something, you’ve
never had, you have to do
something you’ve never done.”*

List of Figures

Figure No.	Figure Caption	Page No.
Figure 1.1	(a) Schematic representation of topology showing smooth deformation from cup to doughnut. (b-e) Are representing genus numbers for different topological systems. (f) Shows that the cut on the doughnut is not changing its Topology.	3
Figure 1.2	Schematic diagram of motion of two electrons having opposite spins with preservation of TRS in TSS.	5
Figure 1.3	(a) Schematic diagram of the Hall effect. (b) Variation of resistivity with the applied magnetic field for classical Hall effect.	7
Figure 1.4	(a) Longitudinal (ρ_{xx}) and transverse resistivity (ρ_{xy}) variation with applied magnetic field, revealing the integer quantum Hall Effect at a very low temperature. (b) Quantization of energy level in discrete Landau Levels with the application of magnetic field by increasing magnetic field strength, only those Landau levels that lie below the Fermi level are occupied.	7
Figure 1.5	(a) Two copies of a QHE edge state for an opposite magnetic field. (b) An amalgamation of these two QHE states creates a quantum spin Hall state without a magnetic field.	10
Figure 1.6	(a) Band structure corresponding to QHE and (b) SQHE are exhibited here. (c) QHE with both right-moving and left-moving edge states that are robust against backscattering. (d) QSHE with upper state right moving spin up and left moving spin down. Backscattering is suppressed from non-magnetic impurities.	10
Figure 1.7	(a) Light waves that are reflected by the top (blue line) and bottom (red line) surfaces of a lens with an antireflection coating interfere destructively, suppressing reflection. (b) Schematic diagram of two opposite scattering paths around an impurity for the QSH state. The 2π total path difference between them results in the suppression of Fermion backscattering.	12

List of Figures

- Figure 1.8** The variation of Hall resistivity ρ_{xy} with the applied magnetic field B . (a) Ordinary Hall effect (b) Anomalous Hall effect, (c) Measured hysteresis loop from quantum anomalous Hall effect. **13**
- Figure 1.9** The schematic diagram to compare the six members of the Hall effect family as (a) ordinary Hall effect, (b) anomalous Hall effect, (c) spin Hall effect (SHE), (d) quantum Hall effect, (e) quantum anomalous Hall effect, and (f) quantum spin Hall effect. **14**
- Figure 1.10** Schematic picture of the band inversion of Bi and Se p orbitals in Bi_2Se_3 at the r point. Stage I represents the effect of chemical bonding, Stage II represents the crystal field splitting, Stage III represents the effect of SOC. **16**
- Figure 1.11** (a) The two time-reversed scattering loops without spin-momentum locking exhibiting weak localization in magnetoconductivity ($\Delta G(B)$). (b) The two time-reversed scattering loops with spin-momentum locking exhibited weak antilocalization in $\Delta G(B)$. **17**
- Figure 1.12** (a) Bulk energy bands for HgTe and CdTe at r point (b) CdTe/HgTe/CdTe quantum well in normal regime $d < d_c$ and in inverted regime $d > d_c$. **21**
- Figure 1.13** (a-b) 2-D and 3-D topological insulators with spin-polarized edge and surface states at the system boundary are shown schematically in real space. (c-d) The development of the 1-D and 2-D Dirac cones is depicted in the energy band diagrams of the 2-D and 3-D topological insulators in momentum space. BCB corresponds to the bulk conduction band, and BVB represents the bulk valence band. **23**
- Figure 1.14** Calculated band structure of Sb_2Se_3 , Sb_2Te_3 , Bi_2Se_3 , and Bi_2Te_3 by ab initio DFT. The occupied bulk and surface states have been represented by red, and the blue color signifies the bulk band gap. **23**
- Figure 1.15** (a) Crystal structure of Bi_2Se_3 , the red box shows single quintuple layer (b) shows that three different A, B, and C sites are assigned to a triangular lattice in one quintuple layer (c) Se and Bi atoms are arranged in a sequence in quintuple. **24**

List of Figures

Figure 1.16	(a) Schematic diagram of Weyl semimetal showing Fermi arc as the surface state. (b) Surface projection of a pair of Weyl cones connecting the Fermi arc. (c) Location of experimentally determined Weyl nodes in the 3-D Brillouin zone and their surface projection.	26
Figure 1.17	Detailed magnetic configurations of (a) a Bloch-type Skyrmion, characterized by a transverse helix with an anticlockwise spin rotation, (b) a Néel-type magnetic Skyrmion, characterized by the anticlockwise-rotated magnetization in a spin cycloid, and (c) a magnetic anti-Skyrmion, characterized by boundary walls that have alternating Bloch and Néel types as one trace around the boundary.	29
Figure 2.1	Flow-chart of single crystal growth technique using modified Bridgeman method is shown with images taken during the process.	32
Figure 2.2	Flow-chart to prepare polycrystals using solid-state reaction technique.	33
Figure 2.3	(a) Schematic of PLD film fabrication mechanism, (b) PLD unit in Department of Physics, IIT (BHU), Varanasi, (c) PLD chamber, (d) PLD chamber when plasma plume is created by a laser pulse, (e) Target material used in PLD, (f) Substrate after deposition.	34
Figure 2.4	The cross-sectional FESEM images corresponding to the (a) Sb_2Te_3 , (b) FeSe and (c) FeSe/ Sb_2Te_3 /FeSe films showing different thicknesses. Thickness vs number of laser shots plotted for (d) Sb_2Te_3 , (e) FeSe and (f) FeSe/ Sb_2Te_3 /FeSe films.	36
Figure 2.5	(a) Photographic demonstration of Bragg's law (b) Actual photograph of Rigaku Mini Flex II DESKTOP X-ray diffractometer set up.	38
Figure 2.6	Schematic of four-probe measurement geometry.	39
Figure 2.7	Schematic diagram for Hall Effect measurement.	41

List of Figures

- Figure 2.8** Schematic diagram of sample holder for thermoelectric measurement. Temperature difference at the both ends of the sample creates a temperature gradient. **42**
- Figure 2.9** (a) Schematic diagram of SQUID-VSM detection system. (b) Photograph of actual QD-MPMS measurement system. **44**
- Figure 2.10** (a) Illustration of Raman effect using energy level diagram. (b) Display the picture of Renishaw micro-Raman spectroscope used in our characterization. (c) Vibrational Raman modes corresponding to Sb_2Te_3 single crystal. **46**
- Figure 2.11** (a) Schematic diagram of a core-level-photoelectron emission process. (b) Hemispherical electron energy analyzer. **49**
- Figure 2.12** (a) Scanning electron microscope' Schematic presentation. (b) Scanning electron microscope (FEI NOVA NANO SEM 450, Courtesy CIFIC IIT BHU) **51**
- Figure 2.13** (a) The schematic arrangements of AFM along with different probing techniques, (b) real image of AFM, NT-MDT Russia. **53**
- Figure 3.1** (a) Raman spectra of Single crystalline $\text{Bi}_{1.9}\text{Dy}_{0.1}\text{Te}_3$ representing the convoluted curves fitted by the Lorentzian line shape function accepting Four optical phonon mode central frequencies at 59, 98, 117, 137 cm^{-1} corresponds to A_{1g}^1 , E_g^2 , A_{1u}^2 and A_{1g}^2 optical modes at 300 K. Inset represents the projection of colour contour corresponding to the temperature-dependent Raman spectra. (b) Temperature-dependent Raman spectra exhibiting the optical phonon modes of the single crystalline $\text{Bi}_{1.9}\text{Dy}_{0.1}\text{Te}_3$ corresponding to 100 K, 150 K, 200 K, 250 K, 273 K and 300 K temperatures. (c) Peak positions of the optical phonon modes showing distinguished red-shift as a function of temperature. (d) Peak intensities of the optical modes increase with rising temperature until 250 K. (e) FWHM of Raman active optical phonon modes are linearly dependent on temperature. (f) Area under the curve of each mode differs with respect to temperature. **63**

List of Figures

- Figure 3.2** Variation of Seebeck coefficient with $\ln(T)$ is displayed in the graph where the red line represents the fitted trajectory of the Semi classical Boltzmann transport theory. Inset manifests the Power Factor of $\text{Bi}_{1.9}\text{Dy}_{0.1}\text{Te}_3$ as the temperature variance. **66**
- Figure 3.3** The calculated values of the figure of merit are represented with respect to temperature. Inset shows the variation of electrical conductivity with temperature. **66**
- Figure 3.4** Electronic and lattice contribution of thermal conductivity as well as the total thermal conductivity is plotted against Temperature. **68**
- Figure 3.5** (a) The optimized cell of $\text{Dy}_2\text{Bi}_{22}\text{Te}_{36}$ of size $2 \times 1 \times 2$ in hexagonal lattice where Dy (blue), Bi (magenta) and Te (green) atoms are represented by filled solid sphere, (b) band structure of pure Bi_2Te_3 calculated without SOC and (c) with SOC effect. The band structure and PDOS of $\text{Dy}_2\text{Bi}_2\text{Te}_3$ are presented in (d) and (e), respectively (calculated with SOC). **71**
- Figure 4.1** (a) Single crystal XRD pattern of the FSBS5 and FSBS10. The cross-sectional FESEM images along with EDX profiles are shown in the insets for both the crystals. (b) The powder XRD of FSBS5 and FSBS10 refined by Rietveld pattern. (c) XRD analysis of the prepared heterostructures compared with the used target materials. (d) Surface and cross-sectional FESEM images of as-prepared heterostructure are exhibited in the left column. The atomic concentration from EDX analysis is shown in the top right table. In the bottom right, the AFM height profile is displayed. **76**
- Figure 4.2** (a) XPS survey scan over the FSBS5, FSBS10 and FS/BS/FS systems. (b-d) represents the elemental XPS spectra of the Bi-4f, Se-3d and Fe-2p for FSBS5 single crystal and (e-g) represents the elemental XPS spectra of the Bi-4f, Se-3d and Fe-2p for FSBS10 single crystal. **80**
- Figure 4.3** (a) XPS atomic percentage profile concerning the etch depth of the FS/BS/FS heterostructure. (b-e) represents the XPS depth profile **80**

List of Figures

- spectra at different etching times for Bi-4f, Se-3d, Fe-2p and Si-2p elements in FS/BS/FS heterostructure, respectively.
- Figure 4.4** (a) and (b) represent the thermal variation of the magnetic moment for FSBS5 and FSBS10, respectively. (c) and (d) exhibits the isothermal moment with varying magnetic fields respectively for FSBS5 and FSBS10. (e, g) and (f, h) demonstrates the real and imaginary part of the ac susceptibility measured at temperature ranging from 2 to 70 K correspondingly for FSBS5 and FSBS10 single crystals. **83**
- Figure 4.5** (a) Represents the thermal variation of the magnetic moment for FS/BS/FS. (b) Exhibits the isothermal moment with varying magnetic fields corresponding to FS/BS/FS heterostructure. (c) MFM image corresponding to the FS/BS/FS heterostructure is showing a clear magnetic domain structure. **84**
- Figure 4.6** (a) Resistivity variation with temperature ranging from 2 to 300 K for FSBS5 and FSBS10 single crystals. Magnetic field dependency of the isothermal magnetoresistance for FSBS5 and FSBS10 are shown in (b) and (c), respectively. We tried to fit the HLN formula in the magnetoconductivity curve below 1 T at 2.5 K for both FSBS5 and FSBS10 as shown correspondingly in the inset of (b) and (c). (d-f) and (g-i) represents the measured hall resistivity with the magnetic field, extracted anomalous hall resistivity with field and the evaluated values of charge density and mobility with temperature for FSBS5 and FSBS10, correspondingly. **86**
- Figure 4.7** (a) Thermal variation of resistivity is exhibited for FS/BS/FS heterostructure. Top-left inset shows the Arrhenius fitted logarithmic value of resistivity. Bottom-right inset shows the linear fitted resistivity data at a temperature range from 280 to 300 K. (b) Kondo model fitted resistance vs temperature in logarithmic scale. Inset represents the $\ln T$ and $T^{1/2}$ fitted resistivity data at very low temperatures. (c) MR (%) plotted from -7 T to 7 T at different temperatures ranging from 2 to 300 K. (d) The isothermal **89**

List of Figures

- magnetoconductivity is fitted with the HLN model below 25 K. (e) The hall resistivity is exhibited from -7 T to 7 T at temperatures ranging from 2 to 300 K. Inset exhibits the mobility variation with charge carrier density. (f) the evaluated values of charge carrier density and mobility are plotted with temperature.
- Figure 4.8** The field-dependent isothermal magnetoconductivity is fitted with the QIE model at temperatures 2 K to 200 K respectively in (a) to (f). The inset of (c) represents the QIE fitted resistivity at low temperature and low magnetic field. The QIE model justified with the resistivity at 300 K is shown in the inset of (f). **96**
- Figure 5.1** The magnetic moment vs. temperature for the heterostructures of different thicknesses. **104**
- Figure 5.2** Magnetic moment variation with magnetic field for the heterostructures of thicknesses (a) 428.8 nm, (b) 271.8 nm, (c) 75.3 nm, (d) 91.9 nm. **104**
- Figure 5.3** The X-Ray Diffraction patterns of as-prepared heterostructures compared with Sb_2Te_3 single crystal and FeSe polycrystal. Inset shows a closer view of the 428.8 nm thick heterostructure. **106**
- Figure 5.4** (a) X-Ray Diffraction spectra of the prepared 75.3 nm thick FeSe/ Sb_2Te_3 /FeSe heterostructures associated with the polycrystalline tetragonal structure of FeSe and single-crystalline rhombohedral structure of Sb_2Te_3 , (b) AFM morphology with the height profile, (c) FESEM image of the 75.3 nm FeSe/ Sb_2Te_3 /FeSe surface showing the grain distribution, (d) EDX spectra of FeSe/ Sb_2Te_3 /FeSe showing atomic profile. **108**
- Figure 5.5** (a) Resistivity variation with temperature ranging from 2 to 300 K. Inset shows Logarithmic plot of resistivity with the inverse of temperature equipped with Arrhenius law, (b) The resistance varying temperature fitted with Kondo model, (c) Hall resistivity variation with the magnetic field at different temperatures. The bottom corner inset attributes the **110**

List of Figures

- dependence of linear mobility on charge carrier density, (d) The temperature dependency of mobility and charge carrier density fitted by double exponential decay.
- Figure 5.6** (a) MR% with magnetic field variation at a temperature ranging from 2 to 300 K, (b) HLN fitted conductivity plot, (c) Magnetic field dependency of MR%. (d) The slope of the linear fitted MR plotted with charge carrier density. The left inset shows the temperature dependency of the slope and the linearly fitted MR% data at above 4 T magnetic field is shown in the right inset. **114**
- Figure 5.7** (a) M-H measured at 5 K temperature. (b) M-H measured at 50 K temperature. (c) M-H loop at 350 K and 580 K temperatures from -3000 to 3000 Oe. Inset illustrates the entire range of the M-H loop at 350 K and 580 K temperatures. (d) M-T plot at ZFC and FC condition from 5 to 700 K. Inset shows the M-T curve for enlarged ZFC and FC showing the transition around 475 K (shaded region). **117**
- Figure 5.8** (a) Raman spectra contain all phonon modes from 100 K to 550 K temperature. (b) Raman line shift and line width plotted against temperature and fitted by AD model for E_g^2 phonon mode. **120**
- Figure 5.9** (a) Raman shifts for A_{1g}^1 , A_{1g}^2 , $E'(Te)$ and $E''(Te)$ vibrational modes. Peak center and FWHM plot with temperature for (b) A_{1g}^1 , (c) A_{1g}^2 , (d) $E'(Te)$ and (e) $E''(Te)$ phonon modes. **123**
- Figure 5.10** (a) Peak center and FWHM plot with temperature for A_{2u}^2 mode. Inset shows the Raman line shift at different temperatures for A_{2u}^2 mode. (b) Three-dimensional colormap of the temperature-dependent Raman spectra denoting all the Raman active modes. **123**
- Figure 5.11** The dependency of AD fitting parameters χ_{c0} and c on the Raman line shift. **124**

List of Figures

- Figure 6.1** Powder XRD patterns corresponding to (a) CSSS, (b) CSSS25 and (c) CSSS50 along with the Rietveld refinement fitted data are shown. (d) Shows the Kagome lattice plane indicating the corner sharing Co atoms with Sn at the center. (e) One unit cell of CSSS lattice presenting all atoms and bonds associated with it. **130**
- Figure 6.2** (a) Temperature-dependent magnetization curves at constant DC fields associated with CSSS. (b) Temperature-dependent inverse DC susceptibility curve fitted with CW law for CSSS. The inset shows the ZFC $M-T$ and corresponding dM/dT vs. T curve exhibiting the transition temperature of the CSSS system. (c) Field dependency of magnetization is exhibited for CSSS at stable temperatures. (d) $M-T$ curves at constant DC fields associated with CSSS25. (e) χ^{-1} vs. T curve fitted with CW law for CSSS25. The inset shows the ZFC $M-T$ and corresponding dM/dT vs. T curve exhibiting the transition temperature of the CSSS25 system. (f) $M-H$ curve is displayed for CSSS25 at stable temperatures. (g) $M-T$ curves at constant DC fields associated with CSSS50. (h) χ^{-1} vs. T curve fitted with CW law for CSSS50. The inset shows the ZFC $M-T$ and corresponding dM/dT vs. T curve exhibiting the transition temperature of the CSSS50 system. (i) $M-H$ curve is displayed for CSSS50 at stable temperatures. **133**
- Figure 6.3** (a), (b) Exhibit frequency dependency on $\chi'_{ac}(T)$ and (c), (d) display $\chi''_{ac}(T)$ curves at different frequencies associated with CSSS. (e), (f) Demonstrate frequency dependency on $\chi'_{ac}(T)$ and (g), (h) show $\chi''_{ac}(T)$ curves at different frequencies associated to CSSS25. (i), (j) Exhibit $\chi'_{ac}(T)$ curves at different constant frequencies and (k), (l) present $\chi''_{ac}(T)$ curves at diverse frequencies for CSSS50. **136**
- Figure 6.4** Dynamic Scaling law fitted freezing temperature versus frequency curves corresponding to (a) CSSS, (b) CSSS25 and (c) CSSS50 are presented. (d), (e) and (f) exhibit f vs T_{fl} curves **137**

List of Figures

following the Vogel-Fulcher model respectively for CSSS, CSSS25 and CSSS50.

- Figure 6.5** (a), (b) Exhibit field dependency on $\chi'_{ac}(T)$ with an inset containing the closer view of χ'_{ac} vs. T below the freezing temperature at different DC bias of CSSS at constant frequency 500 Hz. (c), (d) Display $\chi''_{ac}(T)$ curves at different constant DC fields associated with CSSS with an inset inclosing the larger view of χ''_{ac} vs. T below freezing temperature varying fields. (e), (f) Exhibit the frequency dependency on $\chi'_{ac}(T)$ and $\chi''_{ac}(T)$ respectively at constant DC bias 500 Oe. (g), (h) Demonstrate DC applied field dependency on $\chi'_{ac}(T)$ and (i), (j) show $\chi''_{ac}(T)$ curves varying fields associated to CSSS25. The inset of (g) and (i) display the larger view of the respective curves below the glassy transition. The inset of (h) shows $\chi'_{ac}(T)$ at additional fields. The inset of (j) exhibits $\chi'_{ac}(T)$ at various fields adjacent to T_{f2} . (k), (l) Exhibit $\chi'_{ac}(T)$ curves and (m), (n) present $\chi''_{ac}(T)$ curves at different DC fields associated to CSSS50. (o), (p) and (q) Displays the $d\chi'_{ac}/dT$ with respect to T corresponding to CSSS, CSSS25 and CSSS50, respectively. **138**
- Figure 6.6** DC field dependency on freezing temperature fitted with Almeida - Thouless line for (a) CSSS, (b) CSSS25 and (c) CSSS50 are presented at T_{f1} whereas (d), (e) and (f) exhibits the same at T_{f2} for CSSS, CSSS25 and CSSS50, respectively. **141**
- Figure 6.7** (a) the First quadrant of the $M-H$ curves fitted with the law of approach model for CSSS, CSSS25 and CSSS50 at the lowest temperature 2.2 K. (b) law of approach model fitted on the $M-H$ curves of CSSS50 at the entire range of temperatures below T_C . (c) Temperature dependency of the saturation magnetization and cubic anisotropic constant for CSSS50. **148**
- Figure 6.8** (a) Displays $\chi'_{ac}(H)$ and $\chi''_{ac}(H)$ curves at different temperatures exhibiting diverse magnetic phase boundaries at very low DC applied field for CSSS. (b) Displays $\chi'_{ac}(H)$ and $\chi''_{ac}(H)$ curves varying temperatures corresponding to CSSS25. (c) Displays **150**

List of Figures

temperature dependency on $\chi'_{ac}(H)$ and $\chi''_{ac}(H)$ curves exhibiting unusual magnetic phase boundaries at very low field.

Figure 6.9 *H-T* phase diagrams are demonstrated in (a), (b) and (c) **153**
associated with CSSS, CSSS25 and CSSS50, respectively.

List of Tables

Table No.	Table Caption	Page No.
Table 2.1	The structural parameters of the used substrate and target materials.	35
Table 4.1	Structural parameters evaluated from Rietveld refinement of the powder XRD patterns of the single crystals.	76
Table 4.2	Kondo fitted parameters for the FS/BS/FS system.	90
Table 4.3	HLN fitted parameters for the FS/BS/FS heterostructure.	93
Table 5.1	The thicknesses of the prepared heterostructures are listed with the number of shots.	102
Table 5.2	Statistical parameters assessed from AFM measurement.	109
Table 5.3	Resistance was fitted with the Kondo model below 15 K temperature and the evaluated parameters are listed here.	111
Table 5.4	Arrhenius law fitted parameters over charge carrier density calculated from hall resistivity.	112
Table 5.5	Phase coherence length at different temperatures premeditated using HLN fitting.	114
Table 6.1	The powder XRD refinement parameters correspond to C _{SSS} , C _{SSS25} and C _{SSS50} rhombohedral structure and $R\bar{3}m$ space group.	130
Table 6.2	Parameters determined from the CW equation fitted over the χ^{-1} vs T ZFC data at 500 Oe applied field and the M-H curves corresponding to C _{SSS} , C _{SSS25} and C _{SSS50} systems.	135